$(CUALSE_2)_{1-X}$ $(TASE)_X$ ALLOY SYSTEM ($0 \leq X \leq 0.5$): X-RAY DIFFRACTION, DIFFERENTIAL THERMAL ANALYSIS AND SCANNING ELECTRON MICROSCOPY MEASUREMENTS.

P. Grima-Gallardo[1, 2, 3], M. Muñoz[4], S. Durán[4], G.E. Delgado[5], E. Pérez-Cappé[6], J.A. Aitken[7], D.P. Rai[8]*

1. Centro de Estudios en Semiconductores (CES). Departamento de Física, Facultad de Ciencias, Universidad de Los Andes (ULA). Mérida, Venezuela.
2. Centro Nacional de Tecnologías Ópticas (CNTO). Mérida, Venezuela.
3. Centro de Investigaciones de Astronomía (CIDA). Mérida. Venezuela.
4. Universidad Centro-Occidental "Lisandro Alvarado". Barquisimeto. Venezuela.
5. Laboratorio de Cristalografía, Dpto. Química, Facultad de Ciencias, Universidad de Los Andes. Mérida, Venezuela.
6. Instituto de Ciencia y Tecnología de Materiales (IMRE), Universidad de La Habana, Vedado, Cuba.
7. Department of Chemistry and Biochemistry, Duquesne University, Pittsburgh, USA,
8. Department of Physics, Pachhunga University College, Aizawl, India-796001.

**e-mail: peg1952@gmail.com*

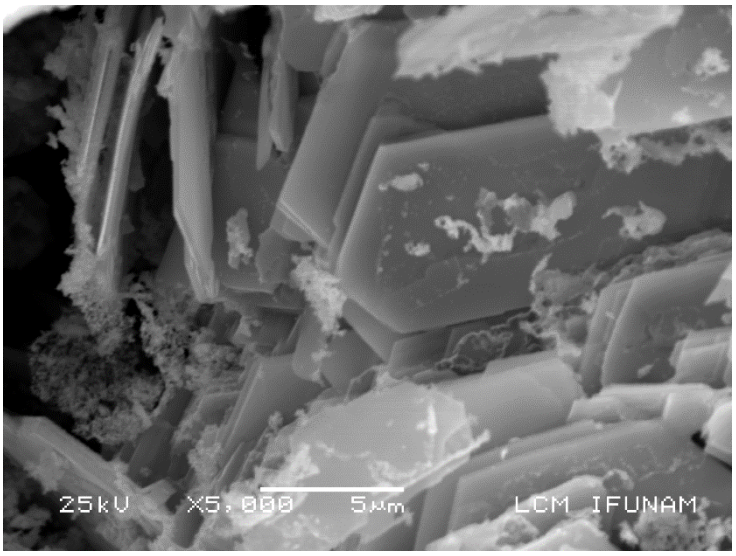

ABSTRACT

Polycrystalline samples belonging to the $(CuAlSe_2)_{1-x}(TaSe)_x$ alloys system, in the composition interval $0 \leq x \leq 0.5$, were synthesized by the melt and anneal method. X-Ray Diffraction (XRD), Scanning Electron Microscopy (SEM), and Differential Thermal Analysis (DTA) techniques were used for the characterization of the products. From XRD it can be observed a chalcopyrite-like single phase in the composition range $0 \leq x \leq 0.1$, with lattice parameters very close to $CuAlSe_2$ and two-phases, chalcopyrite-like and hexagonal-$Cu_{0.52}TaSe_2$, for $0.1 < x \leq 0.5$. By SEM, the stoichiometry for all samples had been measured and the new phase was identified as $(Cu_{0.4}Al_{0.3})TaSe_2$. From DTA the respective phase transitions with temperature were obtained. Using the experimental information, a preliminary T-x phase diagram was proposed.

Keywords*: Alloys, $CuAlSe_2$, TaSe, X-ray diffraction, differential thermal analysis, scanning electron microscopy, phase diagram.*

Recibido: 21-08-2020 ; **Revisado:** 15-10-2020
Aceptado: 15-10-2020 ; **Publicado:** 11-03-2021

pISSN: 0255-6952 | eISSN: 2244-7113
Rev. LatinAm. Metal. Mat. 2021; **41** (1): 34-49

DOI: 10.5281/zenodo.7397075

ALEACIONES DE $(CUALSE_2)_{1-X}$ $(TASE)_X$ $(0 \leq X \leq 0.5)$: MEDIDAS DE DIFFRACCION DE RAYOS X, CALORIMETRIA DIFERENCIAL DE BARRIDO Y MICROSCOPIA ELECTRONICA DE BARRRIDO

RESUMEN

Muestras policristalinas pertenecientes al sistema de aleaciones $(CuAlSe_2)_{1-x}(TaSe)_x$, en el rango de composiciones $0 \leq x \leq 0.5$, fueron sintetizadas usando el método de fusión y recocido. Los productos fueron caracterizados por Difracción de Rayos X (DRX), Microscopía Electrónica de Barrido (SEM) y Análisis Térmico Diferencial (ATD). Los resultados de rayos x muestran la presencia de una única fase en el rango de composiciones $0 \leq x \leq 0.1$, con una estructura cristalina similar al $CuAlSe_2$ y dos fases, calcopirita tipo CuAlSe2 y hexagonal tipo $Cu_{0.52}TaSe_2$, para el rango $0.1 < x \leq 0.5$. Por MEB, la estequiometria de todas las muestras fue medida lo que permitió la identificación de la nueva fase como $(Cu_{0.4}Al_{0.3})TaSe_2$. De los resultados de ATD se obtuvieron los valores de las transiciones de fase en función de la temperatura. Con los resultados experimentales obtenidos se propone un preliminar diagrama de fases T-x.

***Palabras clave**: Aleaciones, $CuAlSe_2$, TaSe, difracción de rayos x, microscopia electrónica de barrido, análisis térmico diferencial, diagrama de fases.*

1. INTRODUCTION

Properties of semiconductors combined with magnetic behavior give place to the so-called diluted magnetic semiconductors (DMS) or "semi-magnetic" semiconductors, largely investigated in the last years due to their possible application in spintronic devices [1]. Usually, preparation of DMS compounds is achieved by substitution of one (or more) non-magnetic element in a semiconductor by magnetic atoms, generally transition metals (TM) as Mn, Fe, Co, Ni, V, Cr, etc., maintaining the empirical Grimm-Somerfield rule of four valence electrons per atomic site [2-3].

$CuAlSe_2$ is a semiconductor material, which crystallize, in the tetragonal structure, space group $I\bar{4}2d$ (N 122), and belonging to the general A^I-B^{III}-C^{VI}_2 family of compounds that have been widely studied [4]. In particular, for its wide direct energy gap (Eg~2.6 eV at 300K) [5] and p-type conduction [6], $CuAlSe_2$ has been considered for blue light-emitting diodes in heterostructures with n-type II-VI semiconductors [7]. Moreover, discovery in the last years of room temperature ferromagnetism (RT-FM) in analogous A^{II}-B^{IV}-C^{V}_2 compounds alloyed with TM has prompted a renewed interest in (A^I-B^{III}-C^{VI}_2) / (TM-VI) alloys [8-9].

On the other hand, Ta is a TM, atomic number 73, electron configuration $[Xe]6s^24f^45d^3$, with a melting point of ~ 4011 K [10]. Due to their high melting point, Ta is usually used to form alloys with desirable properties. Kikkawa *et al* [11] reports that, in the Ta-Se alloy system, they identify two compounds, using Se/Ta composition relations from 2.0 to 3.0: hexagonal $TaSe_2$, space group $P6_3mc$ (N 186) [12] and monoclinic $TaSe_3$, space group $P2_1/m$ (N 11) [13]. They also note that $TaSe_2$ and $TaSe_3$ coexist in the entire range of composition relations, from 2.0 to 3.0, except for Se/Ta = 3.0 for which only $TaSe_3$ was observed. Other authors, (Revelli *et al* [14], Hayashi *et al* [15], and references therein) signal that $TaSe_2$ crystallizes in several different layered polymorphs as a function of temperature. More recently, Ali *et al* [16] studied the synthesis of Ta-based superstructures of intercalated metal dichalcogenides because of their low-dimensional electronic properties leading to the development of charge density waves (CDW) and superconductivity. They reported a new phase entitled 2H-$Cu_{0.52}TaSe_2$ obtained by chemical vapor transport with a hexagonal structure of stacking $TaSe_2$ layers (space group $P\bar{6}m2$) based on the MoS_2 type, with lattice parameters a=3.468 Å and c=13.568 Å. The 2H is referred to as the partial ordering of Cu over the tetrahedral sites, which is responsible for a $2a_0 \times 2b_0 \times c_0$ superstructure.

Concerning (A^I-B^{III}-C^{VI}_2)/(Ta-VI) alloys, up to now our laboratory has been reported the synthesis and characterization of the systems $(CuInSe_2)_{1-x}(TaSe)_x$ ($0 \le x \le 0.5$) [17], $(CuInTe_2)_{1-x}(TaTe)_x$ ($0 \le x \le 1$) [18] and $(CuGaSe_2)_{1-x}(TaSe)_x$ ($0 \le x \le 0.5$) [19]. It was found that the solid solubility of TaSe (or TaTe) was ~ 10% in all alloy systems. In this work, we are investigated the analogous $(CuAlSe_2)_{1-x}$ $(TaSe)_x$ system in the composition range $0 \le x \le 0.5$.

2. EXPERIMENTAL PART

2.1 Synthesis process.

Samples were prepared in steps of x=0.1 in composition from x=0 to 0.5; also, sample x= 1/3 was prepared. Polycrystalline ingots, of about 1 g were obtained by the usual melt and anneal technique, following the procedure described below.

Starting materials (Cu, Al, Ta, and Se) with nominal purity of 99.99 wt. % in the stoichiometric ratio were mixed in an evacuated (10^{-4} Torr) and sealed quartz tube with the inner walls previously carbonized to prevent the chemical reaction of the elements with quartz. The quartz ampoule is heated until 493 K (melting point of Se) keeping this temperature for 48 h and shaking all the time using an electromechanical motor. This procedure guarantees the formation of binary species at low temperatures avoiding the existence of Se free gas at high temperature, which could produce explosions or Se deficiency in the ingot. Then the temperature was slowly increased until 1423 K, with the mechanical shaker always connected for a better mixing of the components. After 24 h, the cooling cycle begins until the anneal temperature (800K) with the mechanical shaker is disconnected. The ampoule is keeping at the annealing temperature for 1 month to assure the thermal equilibrium. Then the furnace is switching off.

2.2 X-Ray Diffraction (XRD).

X-ray powder diffraction data was collected employing a diffractometer (Siemens D5005) equipped with a graphite monochromator (CuK_α, λ = 1.54059 Å) at 40 kV and 20 mA. Silicon powder was used as an external standard. The samples were

scanned from 10–100° 2θ, with a step size of 0.02° and counting time of 20 s. The Bruker analytical software was used to establish the positions of the peaks from the CuKα_1 component and to strip mathematically the CuKα_2 components from each reflection. The peak positions were extracted by means of single-peak profile fitting carried out through the Bruker DIFFRAC^{plus} software. Each reflection was modeled utilizing a pseudo-Voigt function.

2.3 Scanning Electron Microscopy (SEM).

Stoichiometric relations of the samples were investigated by scanning electron microscopy (SEM) technique, using a Hitachi S2500 equipment. The microchemical composition was found by an energy-dispersive x-ray spectrometer (EDS) coupled with a computer-based multichannel analyzer (MCA, Delta III analysis, and Quantex software, Kevex). For the EDS analysis, K_α lines were used. The accelerating voltage was 15 kV. The samples were tilted 35 degrees. A standardless EDS analysis was made with a relative error of ± 5-10% and detection limits of the order of 0.3 wt %, where the k-ratios are based on theoretical standards.

2.4 Differential Thermal Analysis (DTA).

Differential Thermal Analysis (DTA) measurements were carried out in a fully automatic Perkin-Elmer apparatus, which consists in a Khantal resistance furnace (T_{max}=1650 K) equipped with Pt/Pt-Rh thermocouples and an informatics system for the automatic acquisition data. The internal standard used was a high purity (99.99 wt. %) piece of gold. The temperature runs have been performed from ambient temperature to 1400-1500 K, which is the recommended operative limit. The heating rate was controlled electronically to 20 Kh^{-1}; the cooling rate was given by the natural cooling of the furnace after switching off. From the thermogram, transition temperatures were manually obtained from the ΔT vs. T graph with the criteria that the transition occurs at the intersection of the baseline with the slope of the thermal transition peak, as usual. The maximum error committed in the determination of transition temperatures by this method was estimated to be ± 10 K.

3. RESULTS AND DISCUSSION

In figure 1, experimental diffraction patterns are displayed. Sample x=0.1 shows a single chalcopyrite-like phase, with lattice parameters very close to $CuAlSe_2$. The gray ticks signal the position of the peaks and the Miller indices for the *hkl* crystallographic planes are labeled in black color. Samples x=0.2 to 0.4 show the same chalcopyrite-like phase that x=0.1 and traces of secondary phases signaled by red and green ticks. Finally, for sample x=0.5, one of the previous secondary phases (red labels and ticks) becomes the mean phase whereas the chalcopyrite-like phase becomes secondary. Traces of the other secondary phase (green ticks) were also observed and identified as $TaSe_3$.

The phase signaled in red, has been indexed (see Table 1) using the diffraction pattern of sample x=0.5, in a hexagonal structure with the aid of DICVOL 06 software [20], obtaining the lattice parameters: a = (3.454±0.001) Å, c = (13.411±0.003) Å, and V = 138.55 $Å^3$. The indexation was performed with the first 17 diffraction peaks omitting the peaks at a high diffraction angle to obtain the best figure of merit and avoid ambiguity in lattice parameter values. This procedure gives a high figure of merit of 56.7.

However, for a complete identification of the phase crystal structure remains the knowledge of the space group. With this in mind, we remembered that this hexagonal phase has been observed also in the $(CuGaSe_2)_{1-x}$ $(TaSe)_x$ alloys system for sample x=0.5, as is showed in figure 2, where samples x=0.5 for $(CuGaSe_2)_{1-x}$ $(TaSe)_x$ and $(CuAlSe_2)_{1-x}$ $(TaSe)_x$ are compared.

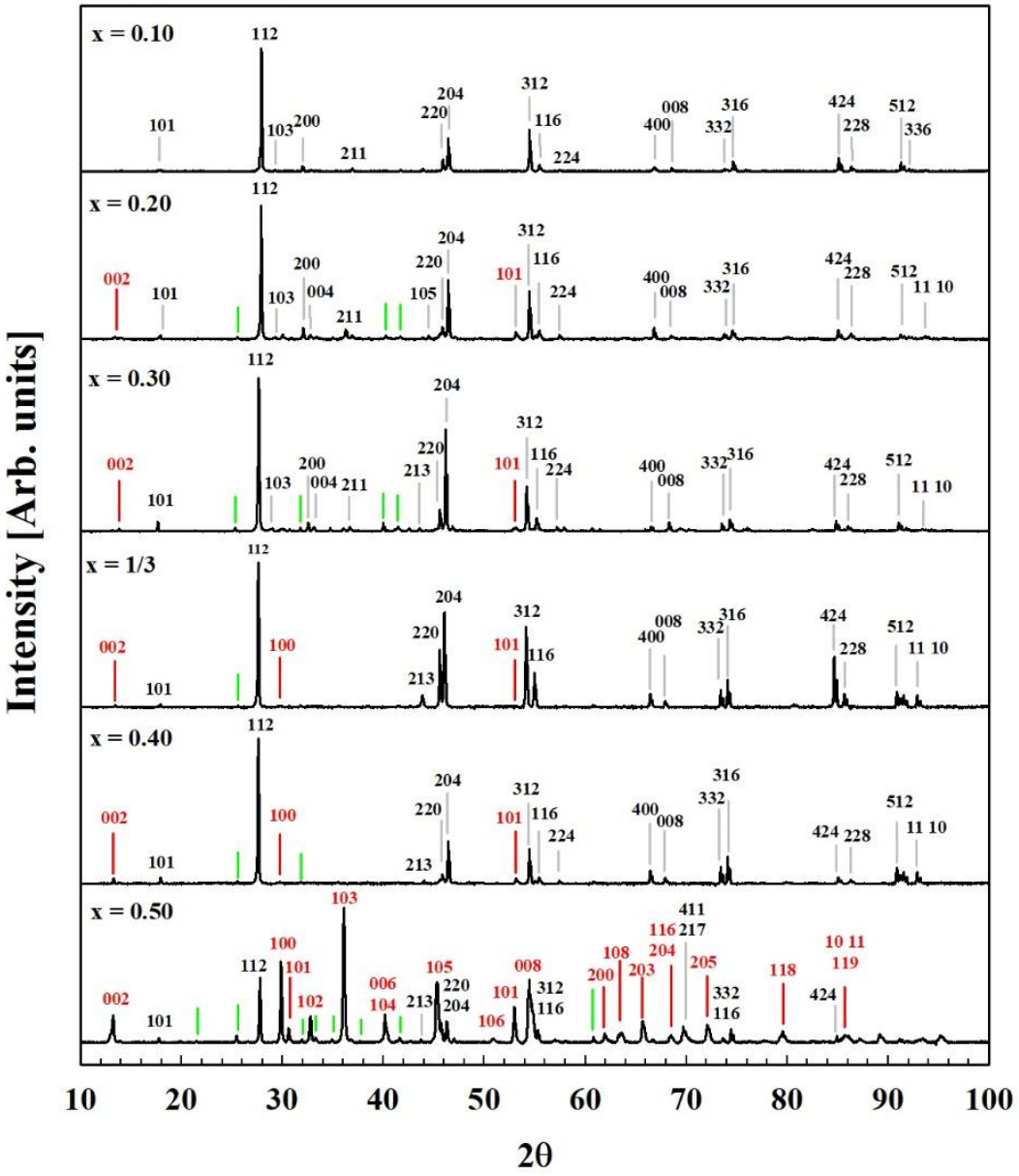

Figure 1. XRD measurements for $(CuAlSe_2)_{1-x}$ (TaSe) x alloys for $0 \leq x \leq 0.5$. The labels in black and gray ticks correspond to a chalcopyrite-like phase, very close to $CuAlSe_2$, whereas red labels and ticks correspond to a hexagonal phase (see text below). The green ticks signal another secondary phase identified as $TaSe_3$.

Table 1. *Indexation of the hexagonal phase (red labels in Figure 1).Direct parameters: a = (3.4539±0.0005) Å, c = (13.4109±0.0026) Å, Volume = 138.55 Å^3.Figures of merit: M (15) = 56.7; F(15) = 25.0(0.0166, 41)*

N	*hkl*	d_{obs} *(Å)*	d_{cal} *(Å)*	*Δd (Å)*	$2\Theta_{obs}$ *(°)*	$2\Theta_{cal}$ *(°)*	*Δ2Θ*	$(I/Io)_{obs}$ *[%]*
1	002	6.68679	6.70489	-0.01811	13.230	13.194	0.036	100
2	100	2.98847	2.99108	-0.00261	29.874	29.847	0.027	43.5
3	101	2.91725	2.91934	-0.00209	30.621	30.599	0.022	7.9
4	102	2.73011	2.73160	-0.00148	32.777	32.759	0.018	15.7
5	103	2.48513	2.48587	-0.00074	36.114	36.103	0.011	88.8
6	006	2.23411	2.23496	-0.00086	40.338	40.322	0.016	11.6
	104		2.23188	0.00223		40.380	0.042	
7	105	1.99662	1.99680	-0.00018	45.387	45.383	0.004	49.8
8	106	1.79012	1.79037	-0.00025	50.974	50.966	0.008	3.5
9	110	1.72669	1.72690	-0.00021	52.989	52.982	0.007	23.1
10	008	1.67624	1.67622	0.00001	54.715	54.715	0.000	6.0
11	200	1.49562	1.49554	0.00008	62.000	62.003	-0.003	2.8
12	108	1.46272	1.46226	0.00046	63.555	63.577	-0.022	7.6
13	203	1.41847	1.41826	0.00020	65.783	65.794	-0.011	9.1
14	116	1.36651	1.36651	0.00000	68.624	68.624	0.000	3.9
	204		1.36580	0.00071		68.665	-0.041	
15	205	1.30657	1.30619	0.00039	72.251	72.276	-0.025	9.0
16	118	1.20313	1.20286	0.00028	79.620	79.642	-0.022	9.6
17	10 11	1.12857	1.12900	-0.00043	86.086	86.045	0.041	10.4
	119		1.12818	0.00038		86.122	-0.036	

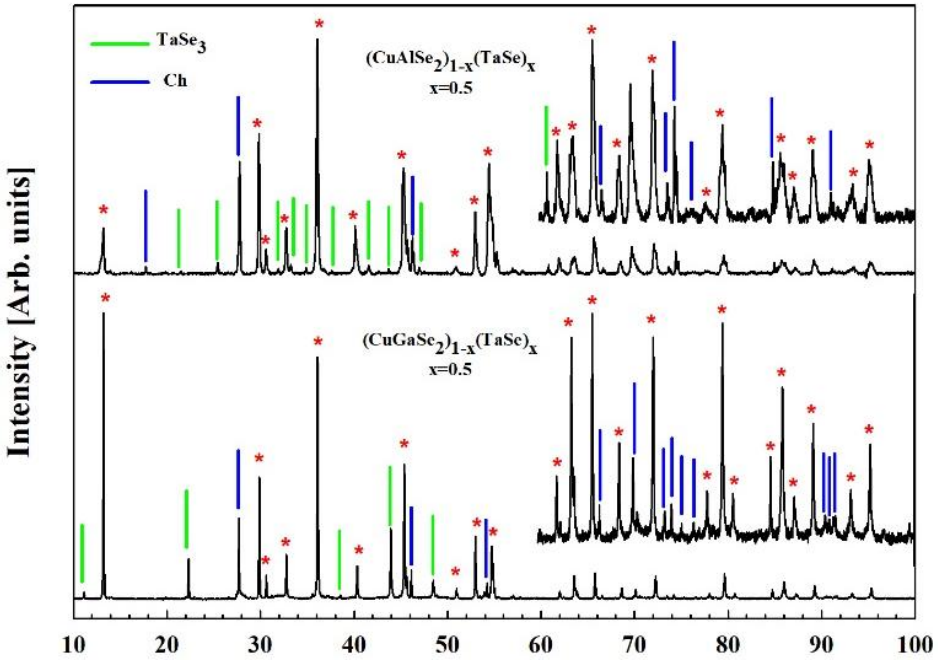

Figure 2. Comparison of samples x=0.5 for $(CuGaSe_2)_{1-x}$ $(TaSe)_x$ and $(CuAlSe_2)_{1-x}$ $(TaSe)_x$ alloys systems. Red asterisks signal the hexagonal phase, blue ticks the chalcopyrite-like phase, and green ticks $TaSe_3$.

There are no dubs than the hexagonal phases observed in both systems are very close. The lattice parameters are nearly the same. The obvious difference is than the hexagonal phase is best defined and the diffraction peaks are stronger and sharper in the system $(CuGaSe_2)_{1-x}$ $(TaSe)_x$. The second step is compared to this well-defined phase with the results obtained recently by Ali *et al* (2014) [16] for intercalated transition metal chalcogenides, in particular the compound 2H-$Cu_{0.52}TaSe_2$. This compound crystallizes in the hexagonal structure, space group $P\bar{6}m2$ (N 187), with lattice parameters *a*=3.468 Å and *c*=13.568 Å which are close to the lattice parameters obtained in our work. In figure 3, we compared the calculated diffraction pattern for 2H-$Cu_{0.52}TaSe_2$ using the mentioned space group, the experimental lattice parameters, and Power Cell software [21] and the experimental diffraction pattern for the sample x=0.5 in the system $(CuGaSe_2)_{1-x}$ $(TaSe)_x$.

The coincidences in the peak positions are very good (the lattice parameters are very close), the only difference occurs in the intensities. This difference can be explained since Cu positions (in $Cu_{0.52}TaSe_2$) are surely shared with Ga in the $(CuGaSe_2)_{1-x}$ $(TaSe)_x$ alloy and the difference in the X-ray mass attenuation coefficients (for CuK_α: 52.9 and 67.9 cm^2/g for Cu and Ga, respectively).

We can conclude that the observed hexagonal phase belongs to the $P\bar{6}m2$ space group with the indexed lattice parameters obtained before. That allows us to perform Rietveld refinements for the full knowledge of their crystal structure which will be the object of the next report in a specialized journal.

Figure 3. Comparison of the experimental diffraction pattern for sample x=0.5 for the alloy system $(CuGaSe_2)_{1-x}$ $(TaSe)_x$

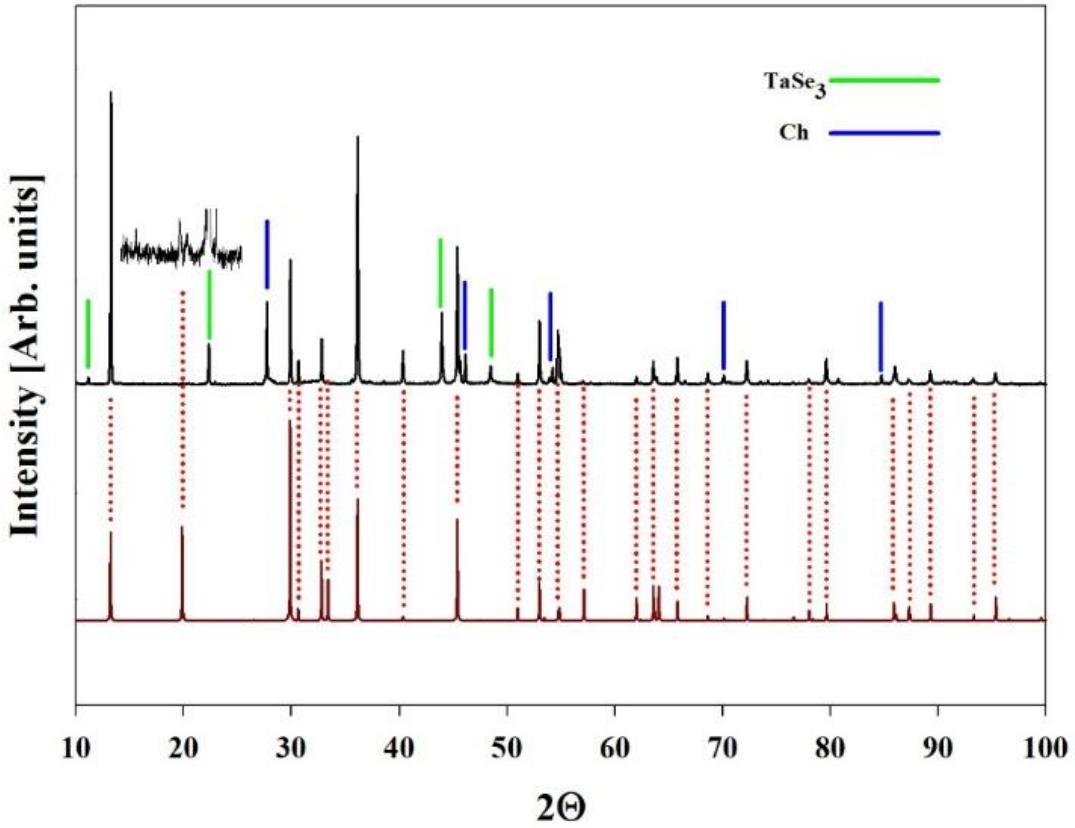

(in the top) with the calculated diffraction pattern for 2H-$Cu_{0.52}TaSe_2$ sample (in the bottom). The insert is an amplification of the particular region. Green ticks: $TaSe_3$ phase; Blue ticks: chalcopyrite $CuAlSe_2$-like phase.

In figure 4, the lattice parameters: *a*, *c*, and *c/a* (tetragonal distortion) for the chalcopyrite-like phase are displayed. At ambient conditions, the values of the lattice parameters of $CuAlSe_2$ are reported to be *a* = (5.617±0.001) Å, *c* = (10.92±0.02) Å and *c/a* = 1.944±0.004 [22]. It can be observed that *a* decrease from x=0 to x=0.2 whereas *c* increases from x=0 to x=0.3 given place to the behavior of the lattice distortion where c/a increases from x=0 to x=0.2. This behavior would be discussed in terms of the disorder that introduces the presence of the third cation (Ta) in the cationic sublattice; it has been well established that the ordered chalcopyrite phase upon disordering tends to the zincblende-like sphalerite phase which is nearly cubic with c/a ~ 2. That is the tendency that we observe until x=0.2. However, for x>0.2, *c/a* decreases suggesting that a reordering of the cationic sublattice occurs.

This reordering is a general tendency of (A^I-B^{III}-C^{VI}_2) / (MT-VI) alloys that we are discussing in other articles, in particular for $(CuInSe_2)_{1-x}$ $(FeSe)_x$ alloys system [23] (see figure 5). The ordered chalcopyrite structure (x=0), space group $I\bar{4}2d$ disorders with the addition of the third cation undergoing a crystallographic transition to the partially disordered chalcopyrite-like phase, space group $P\bar{4}2c$. When the third cation becomes majoritarian (at x=2/3), a new crystallographic phase transition occurs to an ordered stannite, space group $I\bar{4}2m$. In the interval 0 < x < 2/3, the chalcopyrite-like phase has a variable degree of disordering which corresponds to the behavior of the lattice parameters (and also the tetragonal distortion).

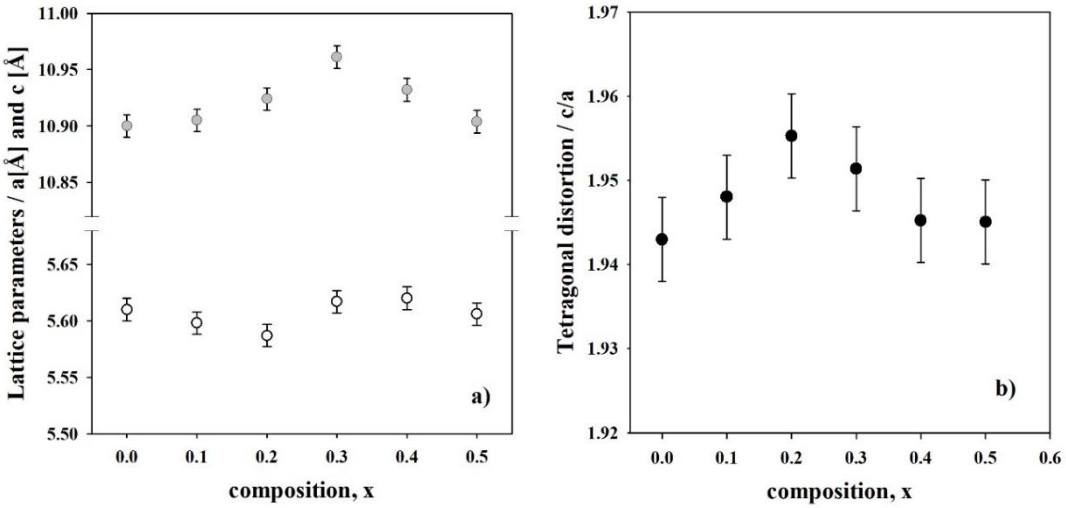

Figure 4. Lattice parameters of $(CuAlSe_2)_{1-x}$ $(TaSe)_x$ alloys for $0 \leq x \leq 0.5$. Left: *a* and *c* parameters; right: tetragonal distortion *c/a*.

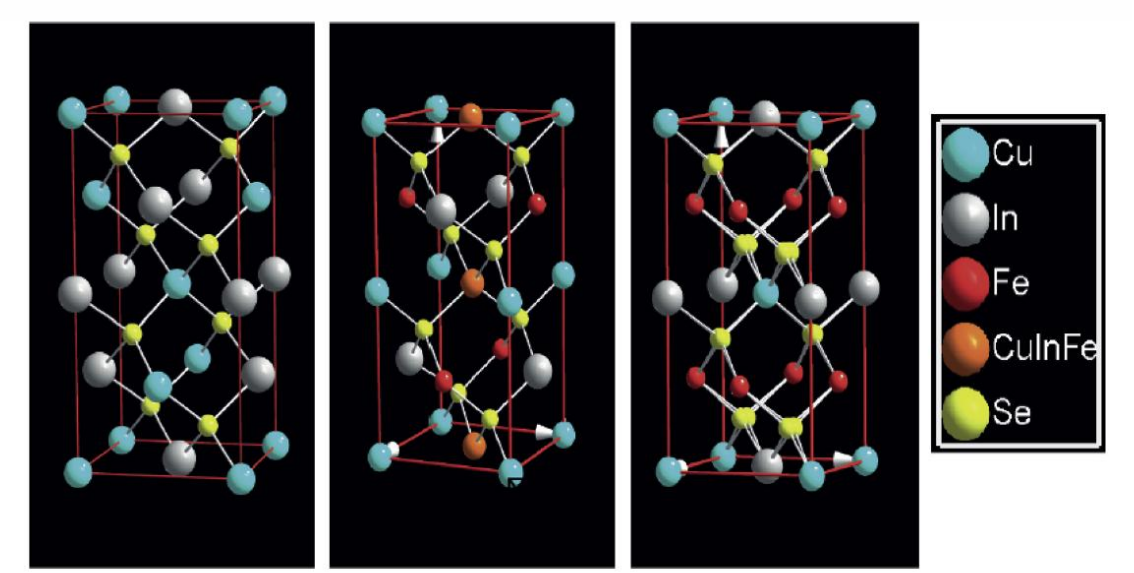

Figure 5. Crystallographic evolution of $(A^{I}\text{-}B^{III}\text{-}C^{VI}2)$ / (MT-VI) alloys using $(CuInSe_2)$ / (FeSe) as example. Left: x=0 $(CuInSe_2)$, ordered chalcopyrite phase, space group $I\bar{4}2d$; center: x=0.5 $(CuFeInSe_3)$, partially disordered chalcopyrite-like phase, space group $P\bar{4}2c$ (note that orange color labeled as CuFeIn represents a crystallographic site that is shared at random by Cu, Fe and In); right: x=2/3 $(CuFe_2InTe_4)$, ordered stannite, space group $I\bar{4}2m$. (For interpretation of the references to color in this figure, the reader is referred to the web version of this article).

In Table 2, SEM results are summarized. Nominal stoichiometry of the chalcopyrite $CuAlSe_2$-like (in red) and $Cu_{0.52}TaSe_2$-like phase (in blue) are compared with experimental measurements.

Ta is always present in the $CuAlSe_2$-like phase but never exceeds 10% as it was observed is similar Ta-based alloy systems [17-19]. $Cu_{0.52}TaSe_2$-like phase has been observed in compositions x=1/3, 0.4, and 0.5 but is not observed for compositions x=0.1, 0.2, and 0.3 although traces were observed in diffraction patterns.

Table 2. *SEM experimental results for $(CuAlSe_2)_{1-x}$ $(TaSe)_x$ alloy system for $0 \leq x \leq 0.5$.*

Composition *x*	*Molecular Weight [gr]*	*Nominal stoichiometry [%]*		*Experimental stoichiometry [%]*	
				$CuAlS_2$-like phase	*$(Cu_{0.52}TaSe_2)$-like phase*
x = 0.0	238.45	Cu=25.0 Al=25.0 Ta=00.0 Se=50.0	---	Cu=25.3 ± 0.2 Al=24.8 ± 0.2 Ta=00.0 Se=49.9 ± 0.5	---
x = 0.1	240.59	Cu=23.7 Al=23.7 Ta=02.6 Se=50.0	Cu=07.4 Al=07.4 Ta=28.4 Se=56.8	Cu = 23.0 ± 0.7 Al = 21.4 ± 0.3 Ta = 01.3 ± 0.5 Se = 54.3 ± 0.5	Not observed
x = 0.2	242.74	Cu=22.2 Al=22.2 Ta=5.6 Se=50.0	Cu=07.4 Al=07.4 Ta=28.4 Se=56.8	Cu = 23.4 ± 0.3 Al = 19.9 ± 0.3 Ta = 02.3 ± 0.8 Se = 54.4 ± 0.4	Not observed
x = 0.3	244.89	Cu=20.6 Al=20.6 Se=50.0 Ta=8.8	Cu=07.4 Al=07.4 Ta=28.4 Se=56.8	Cu = 24.5 ± 0.4 Al = 21.3 ± 0.5 Ta = 03.9 ± 0.8 Se = 50.3 ± 0.7	Not observed
x=1/3	245.60	Cu=20.0 Al=20.0 Ta=10.0 Se=50.0	Cu=07.4 Al=07.4 Ta=28.4 Se=56.8	Cu = 21.5 ± 0.5 Al = 19.3 ± 0.4 Ta = 06.9 ± 0.6 Se = 52.3 ± 0.6	Cu = 08.9 ± 0.3 Al = 07.0 ± 0.5 Ta = 29.7 ± 0.4 Se = 54.4 ± 0.6

x = 0.4	247.03	Cu=18.75	Cu=07.4	Cu = 19.5 ± 0.3	Cu = 10.8 ± 0.3
		Al=18.75	Al=07.4	Al = 19.5 ± 0.4	Al = 07.2 ± 0.5
		Ta=12.5	Ta=28.4	Ta = 06.7 ± 0.7	Ta = 29.8 ± 0.4
		Se=50.0	Se=56.8	Se = 54.3 ± 0.8	Se = 52.2 ± 0.6
x = 0.5	249.18	Cu=16.67	Cu=07.4	Cu = 19.3 ± 0.3	Cu = 09.8 ± 0.3
		Al=16.67	Al=07.4	Al = 19.7 ± 0.3	Al = 07.0 ± 0.5
		Ta=16.67	Ta=28.4	Ta = 05.7 ± 0.5	Ta = 29.8 ± 0.4
		Se=50.0	Se=56.8	Se = 55.3 ± 0.7	Se = 53.4 ± 0.6

The mean experimental stoichiometry observed for the $Cu_{0.52}TaSe_2$-like phase has been calculated as $Cu_{0.4}Al_{0.3}TaSe_2$. In Figure 6, a microphotography of this phase is shown. It can be clearly observed the platelets that confirm the laminar character of the crystal structure of this phase.

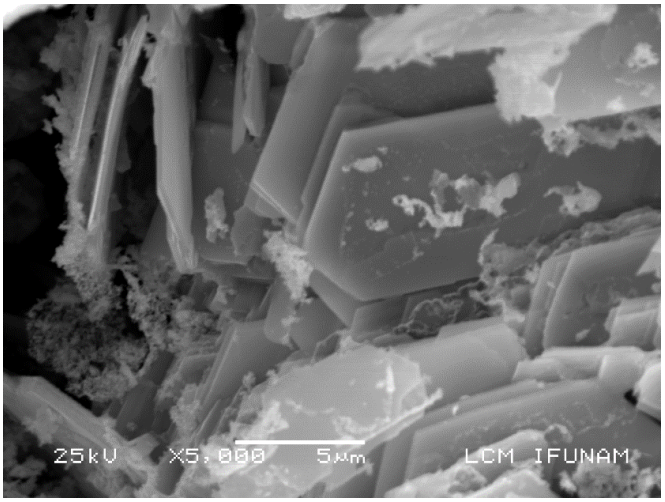

Figure 6. Micrography of the hexagonal $Cu_{0.4}Al_{0.3}TaSe_2$ phase.

Concerning to $CuAlSe_2$, Korzun *et al* [24] reported a melting point of 1363K and no order-disorder transition up to the melting point contrary to other similar A^{I}-B^{III}-C^{VI}_2 compounds. Zunger (1986) [25] proposed a model where the strain energy, set up by the atomic size mismatch between A-C and B-C bonds, control the nature of the state of order, in such a way that displacement parameter (u) parameter (defined in equation 1) can be used to predict the presence (or not) of the order-disorder transition before melting.

$$u - 1/4 = (R_{AC}^2 - R_{BC}^2)/a^2 \quad (1)$$

In this equation, a is the lattice parameter and R the bond distance that can be obtained from the atomic covalent radii (r) through the expressions: $R_{AC} = r_A + r_C$ and $R_{BC} = r_B + r_C$ (A, B and C refers to the atoms A, B and C on A^{I}-B^{III}-C^{VI}_2 nomenclature). Zunger suggests that for a sufficient large displacement parameter, the enthalpy of the disordered phase would be so large, that even the entropy gain upon disordering will be insufficient to stabilize this phase before melting, so the system will be non-disordering. The critical value for u is found to be u~0.265. The model implies that compounds with u > 0.265 must not show order-disorder phase transition whereas compounds for u < 0.265 must disorder before melting. In the case of $CuAlSe_2$, u=0.264, so it must show a disorder phase transition before melting, however, its value has not been reported until now.

In figure 7 (left side), the thermogram for $CuAlSe_2$ obtained from a single crystal growing using chemical transport [5] is displayed, and on the right side the deconvolution of the melting peak. From the thermogram and deconvolution, we observe:

a) In the heating, the melting point at ~1350K and a second peak at ~1287K that we attribute to a solid → solid + liquid transition.

b) In the cooling, a solidification point at 1318K and a second peak at 1145K that we identify to the order-disorder phase transition because of their little size. It is worth to remember that the size

(area under the peak) is the change in the enthalpy (energy) associated to the transition, which is very low for order-disorder transition for chalcopyrite compounds (in de order of 10^{-2} eV/atom) [26]

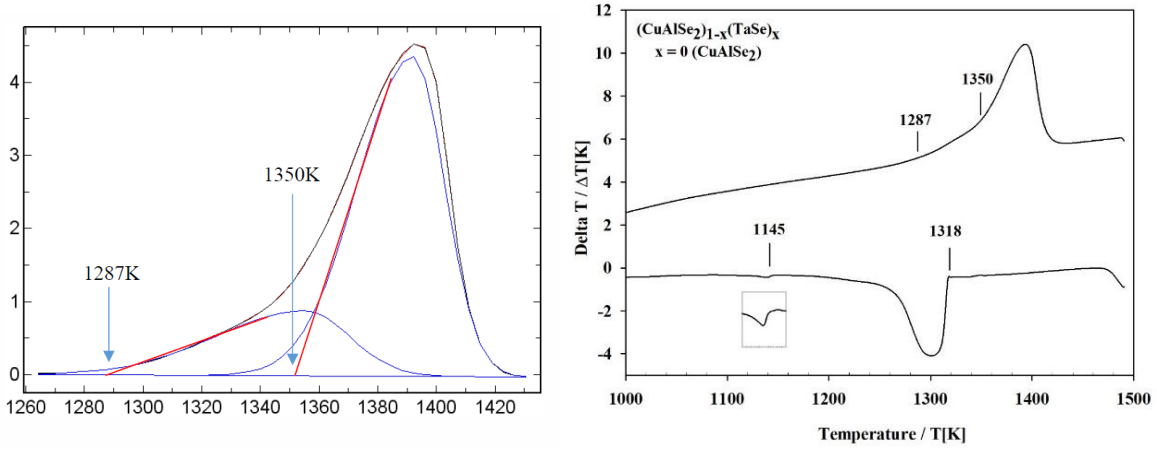

Figure 7. Left side: DTA thermogram for $CuAlSe_2$ single crystal grown by chemical transport method. In the inset, an amplification of the peak at 1145K. Right side: Deconvolution of the melting peak of $CuAlSe_2$. Black: DTA experiment. Blue: fit peaks and baseline. Red: a sum of the two blue peaks. Red lines: extrapolation to the baseline to obtain the transition temperature according to the criteria usually accepted for DTA technique.

The dependence of the critical temperature T_c with composition can be roughly calculated using an extension of the VanVechten theory [27-29]:

$$T_c = \left(\beta\,\Delta Eg + T_0^{0.5}\right)^2 \quad (2)$$

Where β = 43.941 $K^{0.5}$ eV^{-1} and T_0 = 132.64 K are constants obtained from the fit of experimental values; ΔE_g is the variation of the band gap between ordered and disordered phases given by:

$$\Delta E_g = \alpha_{AB} C^2 / A_0 \quad (3)$$

Where A_0 ~ 1 eV is the effective band width parameter, α_{AB} is a correction factor which depends on the involved cations and C is defined as:

$$C = 1.5\, e^2 \left(\frac{Z_B}{r_B} - \frac{Z_A}{r_A}\right) \exp(-kR) \quad (4)$$

A and B denotes the constituent cations of the ternary ABC_2, e is the electron charge, Z represents the valence number of cations, r the covalent radii, k= (4.045 x $10^4/a^{0.5}$) cm^{-1} is the screening wave number related with the lattice parameter of the ternary compound and R = (r_A + r_B + 2r_C)/4 is the arithmetic average of r. The dependence with composition is obtained using:

$$r_A(x) = r_A(1-x) + r_D(x) \quad (5)$$

$$r_B(x) = r_B(1-x) + r_D(x) \quad (6)$$

$$\alpha_{AB}(x) = \alpha_{AB}(1-x-x^2) \quad (7)$$

The values of α_{AB} are known for α_{CuIn}=0.043, α_{CuGa} =0.029, α_{AgIn}=0.039, α_{ZnGe}=0.025 and α_{ZnSn}=0.042, but the value of α_{CuAl} has not been reported yet. Using the former equations and the value of T_c=1145K for $CuAlSe_2$ obtained in this work by DTA, a value of α_{CuAl}=0.019 has been calculated. By simple inspection, it can be noted that the values of α_{AB} are proportional to the sum of the atomic numbers A and B. In figure 8, we are plotted α_{AB} Vs Atomic number A+B, to verify if the obtained value for α_{CuAl} follows this empirical rule. Effectively, it does.

In figure 9, DTA heating and cooling cycles for $(CuAlSe_2)_{1-x}$ $(TaSe)_x$ alloy system in the composition range $0 \leq x \leq 0.5$ are plotted.

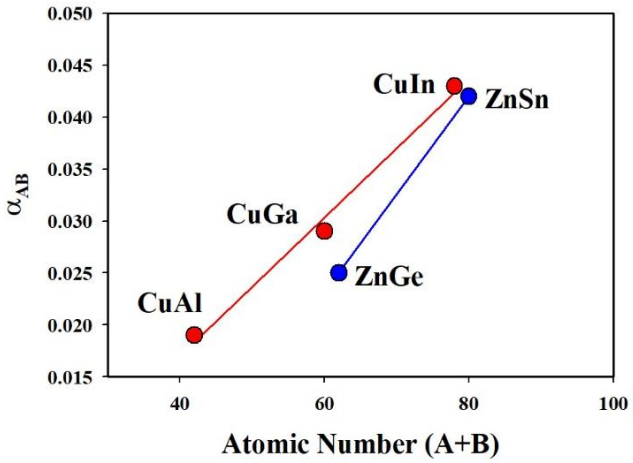

Figure 8. Plot of αAB Vs Atomic number (A+B).

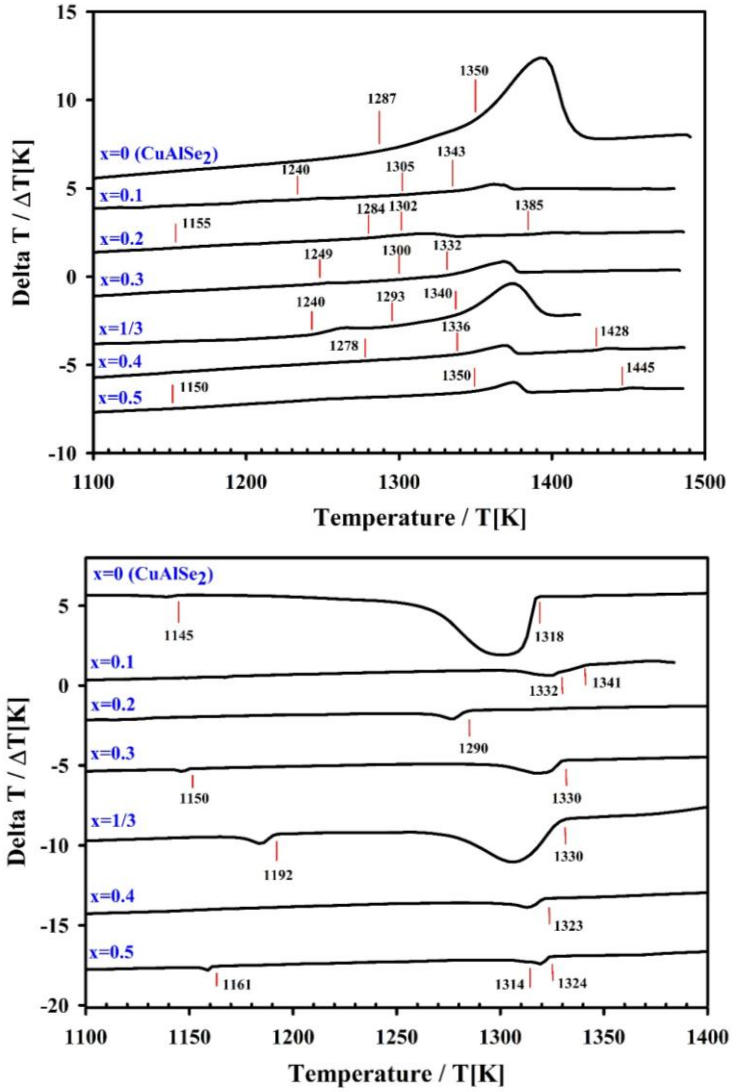

Figure 9. DTA heating (top) and cooling (bottom) cycles for $(CuAlSe_2)_{1-x}$ $(TaSe)_x$ alloys in the composition range $0 \leq x \leq 0.5$. The labels indicated the values of the thermal transition.

A first observation is the reduction of the area under the curve for the melting peak (proportional to the change in enthalpy at the transition) with the increase in composition values, from x=0 to x=0.5, except for x=1/3. It is a fingerprint of the reduction in the energy necessary for melting due to disordering in the cationic sublattice. On the contrary, the increase in the area for x=1/3 suggest a reordering of the cationic sublattice for this composition and an increase in the thermal stability for this composition.

In the heating cycle, all the samples show a peritectic melting point with a relative wide solid + liquid region, except for sample x=0.1 for which the solid + liquid region is narrow. In this cycle, little peaks are also observed at lower temperatures, suggesting solid to solid thermal transitions, however, the peaks are not clear. In the cooling cycle, the liquid to solid + liquid transition is not clear, however, the solid + liquid to solid transition can be observed with high precision as it is usual in this technique. The solid to solid transitions are better observed in the cooling than in the heating cycle. The addition of Ta induces a continuous increase of the melting point of the alloys as it was expected due to its high melting point (4011 K). The synthesis of Ta alloys is possible because of the chemical reaction of Ta with Se at the relatively low temperatures of Se melting (493 K), the procedure used in this work, which allows the formation of binary species ($TaSe_2$ and $TaSe_3$). The presence of a little peak at high temperature, observed for samples x=0.2, 0.4, and 0.5, is due to the presence of one or more (possibly two) liquid + solid regions.

Finally, using all the information, a preliminary T-x phase diagram (see Figure 10) was proposed.

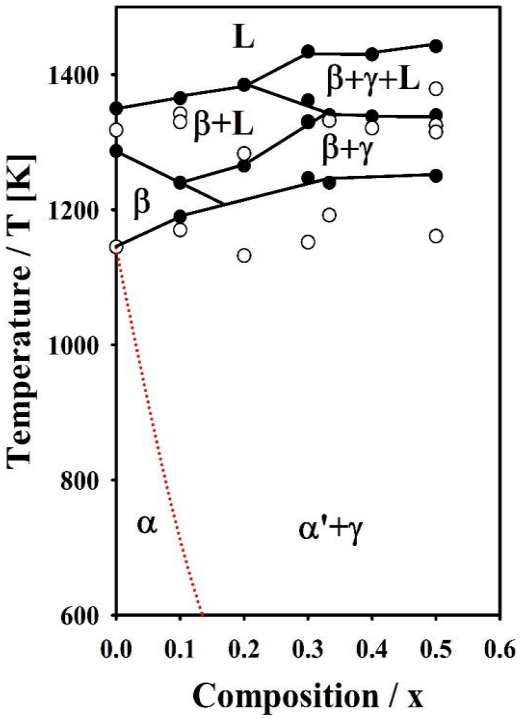

Figure 10. Proposed T-x phase diagram for $(CuAlSe_2)_{1-x}$ (TaSe) x alloy system. The dotted red line was calculated using VanVechten theory (equations 1 to 6). The lecture of the phases is as follows: α (ordered chalcopyrite), α' (partially disordered chalcopyrite), γ (hexagonal $Cu_{0.52}TaSe_2$ -like), β (disordered sphalerite) and L (liquid).

4. CONCLUSIONS

The $(CuAlSe_2)_{1-x}$ $(TaSe)_x$ alloy system has been studied by XRD, DTA, and SEM techniques. It was found that solubility of TaSe in $CuAlSe_2$ is less than 10%, as it was reported for other similar alloy systems as $(CuInSe_2)_{1-x}(TaSe)_x$, $(CuInTe_2)_{1-x}(TaTe)_x$ and $(CuGaSe_2)_{1-x}(TaSe)_x$.

A new phase similar to $Cu_{0.52}TaSe_2$, with experimental stoichiometry close to $Cu_{0.4}Al_{0.4}TaSe_2$, where Cu sites are shared with Al, has been plenty identified; it crystallizes in the hexagonal structure, space group $P\bar{6}m2$ (N 187), with lattice parameters a = (3.4539±0.0005) Å, c = (13.4109±0.0026) Å and Volume = 138.55 $Å^3$. Concerning to $CuAlSe_2$, two new thermal phase transitions were observed: an order-disorder at 1145 K and solid to solid + liquid at 1287 K. From the temperature value of the order-disorder transition, the value of the parameter $\alpha_{Cu\text{-}Al}$ = 0.019 in the VanVechten's model was obtained. Finally, a first version of the T-x phase diagram for this alloy system was reported.

5. ACKNOWLEDGMENTS

We are very grateful to Dr. Dwight Acosta, Institute of Physics, Universidad Autónoma de México (UNAM) for SEM measurements.

6. REFERENCES

[1]. Jain M. Diluted Magnetic Semiconductors. World Scientific, Singapore, 1991. For a review of fundamental properties, see Galazka R.R., in Proceedings of the 14th International Conference of the Physics of Semiconductors, Edinburgh, 1978, edited by B.L.H. Wilson (IOP Bristol, 1979), p. 133; and Furdyna J.K. J. Appl. Phys. 53, 7637 (1982). For a review about Spintronics see: Pearton S.J., Abernathy C.R., Norton D.P., Hebard A.F., Park Y.D., Boatner L.A. and Budai J.D. (2003). Advances in wide bandgap materials for semiconductor spintronics. Materials Science and Engineering R40, 137-168.

[2]. Parthé E. "Intermetallic compounds, principles and applications", John Wiley & Sons, Chichester, UK. 1995; Vol. 1.

[3]. Wyckoff RWG. "Crystal Structures". Interscience Publishers. John Wiley & Sons, Chichester, UK. 1965; Vol. 1.

[4]. Shay JL, Wernick JH., "Ternary Chalcopyrite Semiconductors: Growth, Electronic Properties, and Applications", Pergamon Press, Oxford, 1974.

[5]. Roa L, Grima-Gallardo P, González J, Chervin JC, Itié JP, Chevy A. Cryst. Res. Technol. 1996; 31: 49-52.

[6]. Chichibu S, Shishikura M, Ino J, Matsumoto S. J. Appl. Phys. 1991; 70, 1648-1653.

[7]. Roa L, Chervin JC, Chevy A, Grima-Gallardo P, González J. 11th Int. Conf. on Ternary and Multinary Compounds, ICTMC-11, Saldford, 8-12 September 1997. 519-522.

[8]. Grima-Gallardo P, Méndez L, Delgado GE, Cabrera H, Pérez-Cappé E, Zumeta-Dubé I, Rodríguez A, Aitken JA, Rai DP. Int. J. Exp. Spectroscopic. Tech. 2018; 3: 16-26.

[9]. For a review of room temperature, ferromagnetic semiconductors: Gupta A. "Novel room temperature semiconductors". Doctoral Dissertation. Royal Institute of Technology. Dept. of Materials Science and Engineering. Division of Engineering Materials Physics. Stockholm. Sweden. This paper is available at htpp://repositories.cdlib.org/lbnI/LBNL-56596. University of California, (2004).

[10]. National Institute of Standards and Technology. Technology Administration, U.S. Department of Commerce.

[11]. Kikkawa S, Shinya K, Koizumi MJ. Solid State Chemistry 1982; 41: 323-328.

[12]. 74-0604 International Center for Diffraction Data (ICDD) 2002.

[13]. 18-1310 International Center for Diffraction Data (ICDD) 2002.

[14]. Revelli JF, Phillips WA. J. Solid State Chemistry. 1974; 9: 176-186

[15]. Hayashi K, Tanico Y, Kawachi K, Nakata Y, Inoue K, Maeda NJ. Alloys and Compounds. 2007; 442: 117-118

[16]. Ali SI, Mondal S, Prathapa SJ, Van Smaalen S, Zorb S, Harbrecht B. Z. Anorg. Allg. Chem. 2012; 638: 2625–2631. See also Ali SI. PhD Thesis "Synthesis, Superstructure, Vacancy-Ordering of Intercalated Transition Metal Di-chalcogenides", Beirut University (Lebanon) 2014.

[17]. Grima-Gallardo P, Méndez L, Delgado GE, Cabrera H, Pérez-Cappé E, Zumeta-Dubé I, Rodríguez A, Aitken JA, Rai DP. Int. J. Exp. Spectroscopic. Tech. 2018; 3: 16-26.

[18]. Grima-Gallardo P, Izarra O, Méndez L, Torres S, Quintero M, Cabrera H, Pérez-Cappé E, Zumeta-Dubé I, Rodríguez A, Aitken JA. Rai DP. Journal of Alloys and Compounds. 2018; 747: 176-188.

[19]. Grima-Gallardo P, Muñoz M, Durán S, Delgado GE, Pérez-Cappé E, Aitken JA, Senhri Journal of Multi-disciplinary Studies 2020; 5(1): 1-18.

[20]. Boultif A, Louer DJ. Appl. Cryst. 2004; 37: 724-731.

[21]. http://www.ccp14.ac.uk/ccp/web-mirrors/powdcell/a_v/v_1/powder/e_cell.html

[22]. CRC Handbook of Chemistry and Physics. David R. Lide. 79th Edition, CRS Press, Boca Raton, Florida (1998).

[23]. Grima-Gallardo P, Torres S, Quintero M, Nieves L, Moreno E, Delgado GE. Journal of Alloys and Compounds. 2015; 630: 146–150.

[24]. Korzun BV, Fadzeyeva AA, Bente K, Schmitz W, Komnichan G. Phys. Stat. Sol. (b). 2005; 242:1581-1587.

[25]. Zunger A. Appl. Phys. Lett. 1986; 50(3): 164-166.

[26]. Wei SH, Ferreira LG, Zunger A. Phys. Rev. 1992; B45: 2533- 2536.

[27]. VanVechten JA., "Ternary and Multinary Compounds", Materials Research Society, 1987, p. 423.

[28]. Rincon C. Phys. Rev. 1992; B45: 12716.

[29]. Grima-Gallardo P, Phys. Status Solidi (a). 1992; 134: 119-125.

7. MINIBIOGRAFÍA DE AUTORES.

PEDRO GRIMA GALLARDO. Doctorat in Science des Matériaux, Université Pierre et Marie Curie (Paris VI). France. President of the Centro de Investigaciones de Astronomía (CIDA) and the Centro Nacional de Tecnologías Ópticas (CNTO), Mérida, Venezuela. Field of specialty: X-ray diffraction at high pressure and high temperature, Semiconductor alloys, Spintronics, Solar Cells.
ORCID: 0000-0003-4342-8069

EDUARDO LÁZARO PÉREZ CAPPÉ Doctor in Chemical Sciences from the Universidad de La Habana. Titular Researcher at the Universidad de La Habana. Specialist in Material Characterizations, Electrical and Electrochemical Properties, Nanotecnology, Thermal Properties.
ORCID: 0000-0001-7842-2770

GERZON E. DELGADO. Titular Professor, Departamento de Química, Universidad de Los Andes (ULA). His research focuses Materials Science, Solid State Physics and Chemistry, Structural Chemistry, Crystallography, Structural Studies in different materials using X-ray diffraction techniques in mono and polycrystalline samples.
ORCID: 0000-0003-3970-2387

JENNIFER A. AITKEN. Professor Bayer School of Natural and Environmental Sciences Chemistry & Biochemistry. Ph D. Michigan State University. Research: Solid-State Inorganic Materials Chemistry; New Diamond-like Semiconductors with novel Magnetic and Optical Properties; Diluted Magnetic Semiconductors; Development of a new class of Solid-State Compounds.
ORCID: 0000-0001-8281-5091

DIBYA P. RAI. Dr. Dibya Prakash Rai completed his MSc (2009) and received PhD in Physics, from Mizoram University, India in 2013 under the supervision of Professor R. K. Thapa. His research focuses on the theoretical investigation of electronic, magnetic and thermoelectric properties of Heussler Alloys using density functional theory (DFT). His research works also extended to 2D nanomaterials for energy storage and energy harvest.
ORCID: 0000-0002-3803-8923

MARCOS MUÑOZ-PINTO. Doctor in Materials Science, Universidad de Los Andes, Venezuela. Researcher and Physics teacher at Universidad Centro Occidental "Lisandro Alvarado" (UCLA). Field of research: Semiconductors, Semiconductor Alloys, phase diagrams.
ORCID: 0000-0002-1870-1150

SONIA DURÁN-PIÑA. Doctor in Materials Science, Universidad de Los Andes, Venezuela. Researcher and Physics teacher at Universidad Centro Occidental "Lisandro Alvarado" (UCLA). Field of research: Semiconductors, Semiconductor Alloys, phase diagrams.
ORCID: 0000-0003-4856-6946